

Splitting in the Fermi surface of ZrTe₃: A surface charge density wave systemMoritz Hoesch,^{1,*} Xiaoyu Cui,^{2,†} Kenya Shimada,² Corsin Battaglia,³ Shin-ichi Fujimori,⁴ and Helmuth Berger⁵¹*European Synchrotron Radiation Facility, 6 rue Jules Horowitz, 38043 Grenoble Cedex, France*²*Hiroshima Synchrotron Radiation Centre, Hiroshima University, Kagamiyama 2-313, Higashi-Hiroshima 739-0046, Japan*³*Institut de Physique, Université de Neuchâtel, 2000 Neuchâtel, Switzerland*⁴*Synchrotron Radiation Research Unit, Japan Atomic Energy Agency, Mikazuki, Hyogo 679-5148, Japan*⁵*Institut de Physique de la Matière Complexe, Ecole Polytechnique Fédérale de Lausanne, 1015 Lausanne, Switzerland*

(Received 6 February 2009; revised manuscript received 5 June 2009; published 18 August 2009)

The electronic band structure and Fermi surface of ZrTe₃ was determined by angle-resolved photoemission spectroscopy. Several bands and a large part of the Fermi surface are found to be split by 100–200 meV into two parallel dispersions. Calculations of the bulk band structure cannot reproduce this splitting even if spin-orbit interaction is taken into account. A bilayer model representing the top layers of a surface-relaxed structure without reconstruction introduces the observed splitting and reproduces most features observed in the data thus suggesting a surface relaxation of the freshly cleaved ZrTe₃. The dispersion of the highly nested small electron pocket that gives rise to the charge density wave is traceable even in the low-temperature gapped state and the gap energy is determined as $\epsilon_g = 65 \pm 10$ meV.

DOI: [10.1103/PhysRevB.80.075423](https://doi.org/10.1103/PhysRevB.80.075423)

PACS number(s): 73.20.-r

I. INTRODUCTION

In a one-dimensional (1D) metal the atoms form chains and specific electronic states are confined to travel predominantly along these chains. This leads to a Fermi surface (FS) topography that is characterized by parallel sheets as the band dispersion is significant only along the chain direction. The corresponding FS nesting makes the system susceptible to instabilities such as spin or charge density waves (SDW or CDW), if assisted by a coupling to the respective magnetic or lattice degrees of freedom. Chainlike arrangements are found in a number of crystal structures and CDW phenomena are observed in varied systems such as blue bronze, the platinum chain compound (KCP), (TaSe₄)₂I, and the prismatic chains of NbSe₃ and TaS₃.¹ The ideal CDW should be an isolated Peierls chain, but in a crystal a certain coupling between parallel chains is always present. Reduced coupling of adjacent chains is achieved in surface CDW systems such as In/Si(111),² which has nested Fermi surface sheets and opens a gap at $T=120$ K and the recently discovered Au/Ge(001).³ Electron correlations can drive the formation of even more complex and competing ground states other than the CDW.

To date it is still very difficult to predict whether a material will exhibit a CDW. Fermi surface nesting is certainly an important ingredient and can be studied by ground-state electronic structure calculations of the unmodulated structure. The formation of a statically modulated CDW ground state requires a certain coupling between the chains so that below the Peierls transition a three-dimensionally (3D) ordered ground state can exist. Phonons eventually destroy the CDW order at the Peierls transition temperatures, but on the other hand the electron-phonon coupling (EPC) is also needed to assist the formation of a static distortion where the lattice degrees of freedom follow the electronic modulation. It is thus highly interesting to study how the CDW reacts to slight changes in the chain structure and coupling, which can be induced by pressure,⁴ strain, or, in the case discussed in this paper, by the presence of the surface.

We present an extended data set of photoelectron spectroscopy data of the layered material ZrTe₃. A cleaved surface of a van der Waals bonded layered system is usually assumed to have a bulklike termination and the absence of dangling bonds makes the formation of surface states unlikely. Thus the surface-sensitive photoelectron signal is often regarded as representative of the bulk electronic structure. Indeed, in ZrTe₃ a previous photoelectron spectroscopy study⁵ found the momentum structure of the charge density wave and its temperature dependence in good agreement with the complementary and less surface-sensitive optical conductivity data.⁶ We find, however, that our data are not compatible with the expected features of the bulk electronic structure and conclude that the signal, as well as the results of other studies,^{5,7,8} represent a special surface system that is modified from the bulk structure, with the interesting consequence that this modified system shows potential differences to the related bulk of ZrTe₃.

In the bulk, the CDW transition of ZrTe₃ is well characterized. It was first observed as a resistivity anomaly at $T_{CDW}=63$ K for measurements along the crystal a and c directions.⁹ The periodic lattice distortion was observed by diffraction¹⁰ and by a giant Kohn anomaly behavior of a soft phonon.¹¹ Below T_{CDW} the system is left in a metallic state, where superconducting filaments emerge at very low T ($T_c = 2$ K).^{4,9} The opening of a gap in the electronic structure does not affect the entire Fermi surface. In fact, the Fermi surface consists of at least two principal sheets [Fig. 1(c)] as seen in calculations^{12,13} and experiments.^{5,7,14} A central 3D Fermi surface is derived from holes that propagate mostly along the prismatic (ZrTe₃)_∞ chains along the b direction. The elongated cross section in the a^*-b^* plane allows for a certain nesting along b^* . A much better nesting condition is found in the small electron pocket of the Te $5p_x$ band which propagates along the Te-Te chains formed by the lateral bonding of adjacent prisms. This quasi-one-dimensional (q1D) Fermi surface with principal propagation direction along a was identified to match the observed modulation vector $q_{CDW}=(0.07,0,0.333)$.¹⁰ Strictly speaking, the q1D

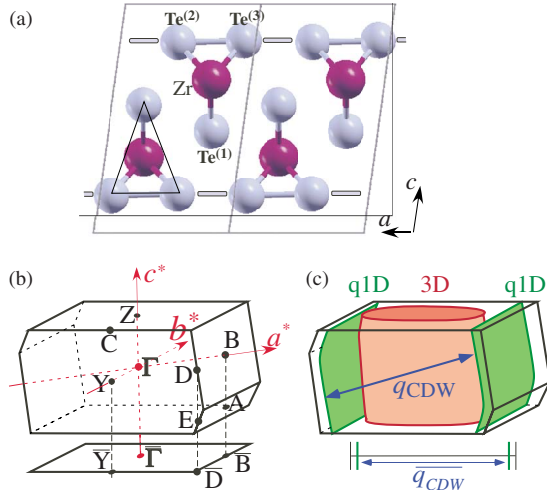


FIG. 1. (Color online) (a) Projection of the unit cell onto the a - c plane of the structure showing the chains in the Te layer adjacent to the van der Waals gap. (b) First Brillouin zone of the monoclinic structure and surface Brillouin zone (SBZ). (c) Schematic representation of the two main sheets of the Fermi surface with the nesting vector. $\overline{q_{CDW}}$ represents the projection of q_{CDW} onto the SBZ.

FS consists of two sheets due to the inequivalence of the two Te atoms in the Te-Te chains. In the out-of-plane direction c the structure is much more weakly bonded since only van der Waals forces act between layers. The band dispersion is consequently much weaker. Some dispersion has, however, been predicted by all calculations. In particular the q1D Fermi surface can be seen to follow the inclination of the Brillouin zone boundary (BZB) given by the monoclinic $P2_1/m$ structure.¹²

The Te layer adjacent to the van der Waals gap is of special interest. It is formed by the inequivalent but almost equidistant Te⁽²⁾ and Te⁽³⁾ atoms and its band structure has been discussed in Ref. 12. Due to the weak bonding it is the most likely surface termination layer in a cleaved sample. The nesting $\overline{q_{CDW}}$ of the artificial two-dimensional (2D) single layer would be along the $\overline{\Gamma-B}$ direction.

This paper is organized as follows: in the next section we detail the experimental procedure and computational details. Sec. III shows the measured data and discusses the observed band dispersions and splittings. Sec. IV discusses the implications of the observed splitting through comparison with calculations. Sec. V reports on the observations concerning the CDW gap. The conclusions are summarized in the final section.

II. EXPERIMENT AND CALCULATIONS

Single crystals of ZrTe₃ were grown by vapor-phase transport in the form of large shiny platelets. Photoemission data were acquired from samples freshly cleaved at room temperature by peeling off the top layers with Scotch™-tape. In an ultrahigh vacuum of typical residual pressure 2×10^{-10} mbar the samples remained clean and sharp spectra could be acquired over a two days period following cleavage. The sample normal and high-symmetry directions were

determined from the shape of the sample, the direction of the fibers along the b axis and the symmetry of photoemission angular scans. The Fermi level and the total-energy resolution ($\Delta E=17$ meV) were determined from the metallic Fermi cutoff of a polycrystalline gold film.

The angle-resolved photoelectron spectroscopy (ARPES) experiments were performed at the linearly polarized undulator beamline BL-1 at the Hiroshima Synchrotron Radiation Centre.¹⁵ The experimental station is equipped with a low-temperature two-axis goniometer. The angle-dispersive detection direction of the electron spectrometer is in the plane of linear polarization of the photons. Additional data were acquired using a similar setup with even higher resolution at the Swiss Light Source using elliptically polarized light (Figs. 4 and 7). Mapping of the photoelectron angular distribution to momentum k_{\parallel} was performed according to standard parallel projections. The locus of the Brillouin zone boundaries was determined from the symmetry of the data sets.

Two distinct sample mountings were employed that lead to different orientations of the polarization vector with respect to the sample. With the b axis mounted horizontally the central 3D Fermi surface was accurately mapped since the tilt corresponds to the direction $\overline{\Gamma-B}$. No mirror plane of bulk ZrTe₃ is present in these scans, but states that are odd in a are suppressed in this sample orientation. With the b axis mounted vertically, the q1D Fermi surface and the \overline{B} point (where the two principal sheets approach) are accurately mapped. Here the selection rule implies that at the \overline{B} point only even states with respect to the a - c plane are observable.

Peak positions, intensities and widths were extracted from the measured data using model functions consisting of two or four Lorentzians. In the case of momentum distribution curves (MDC) at constant binding energy, the widths of the Lorentzians were restricted to be equal for equivalent bands and a constant background was included in the fit function. Typical widths were on the order of 0.07 \AA^{-1} (0.03 \AA^{-1} for the higher resolution data sets). In the case of energy distribution curves (EDC) at constant position in momentum space, the resulting sum of Lorentzians and a linear background was multiplied by a Fermi distribution function with a predetermined Fermi energy and an effective temperature (width of the Fermi cutoff) that takes into account the finite-energy resolution. Typical widths of EDC features ranged from 70 up to 120 meV for very steep bands, where the momentum resolution has an effect on the spectral widths.

Ab initio band-structure calculations were performed using the WIEN2K code.¹⁶ For bulk ZrTe₃ the crystal structure from the literature¹³ was optimized until the forces on all atoms converged below a limit of 2 mRy/Bohr. The augmented plane-wave basis was expanded to a wave-number limit k_{\max} given by $r \cdot k_{\max} = 7$, where $r=2.5$ Bohr is the radius of the atomic spheres. The total energy was integrated over a momentum space mesh of $13 \times 19 \times 7$ points which was reduced according to the crystal symmetries. For a calculation in a slab geometry the unit cell was doubled in the c direction and a vacuum layer of 10 Bohr thickness was inserted. The two-dimensional electronic structure was calculated on a $26 \times 40 \times 1$ mesh and the atomic positions were relaxed to less than 2 mRy/Bohr resulting in slightly ex-

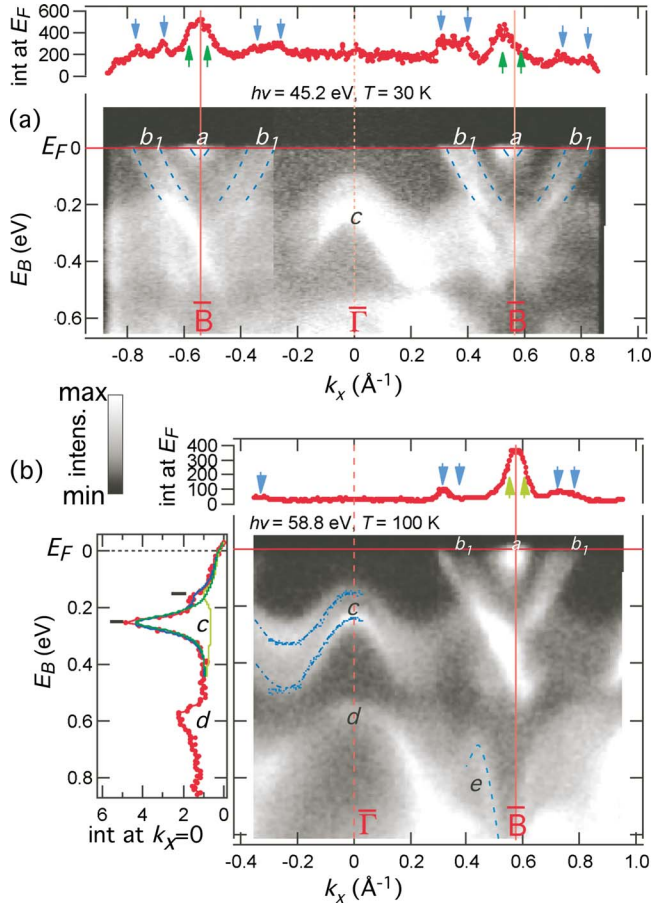


FIG. 2. (Color online) ARPES dispersion maps along the direction $\bar{\Gamma}$ - \bar{B} measured with photon energies (a) $h\nu=42.5$ eV and (b) $h\nu=58.8$ eV at low temperatures as indicated. Dots in the left section of (b) are peak positions from peak fitting. Dashed lines mark the observed dispersions in selected regions as a guide for the eye. The top of each panel shows the intensity distribution at E_F with the peak positions marked by arrows.

panded layers. Other calculation parameters were identical to the bulk calculation. Fermi surface cuts were interpolated from the Fermi level crossings of all bands in a regular 40×20 grid in the symmetry-reduced part of the first Brillouin zone.

III. BAND DISPERSIONS AND SPLITTINGS

Dispersion maps at two photon energies across $\bar{\Gamma}$ in the a - c mirror plane are shown in Fig. 2. The photoemission intensity is plotted on a linear gray scale versus the binding energy E_B and the wave vector k_x along $\bar{\Gamma}$ - \bar{B} . The two data sets differ in sample temperature T and photon energy $h\nu$. Further data sets have been acquired in the photon energy range $h\nu=36.7$ - 56.8 eV. As the total momentum of the photoelectrons is varied with their energy a signature of the dispersion k_{\perp} along c^* is expected. However, except for variations in the relative intensity, the observed bands, their binding energies and dispersion match between all the data sets. Thus the data represent the two-dimensional electronic structure of a ZrTe_3 layer.

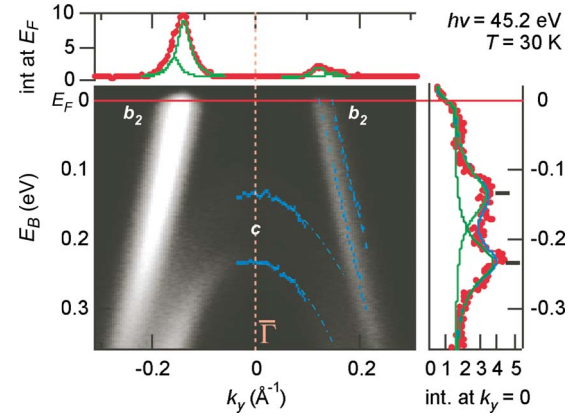


FIG. 3. (Color online) ARPES dispersion map along $\bar{\Gamma}$ - \bar{Y} measured with $h\nu=42.5$ eV and $T=30$ K. The top section shows the intensity distribution at E_F . Dots are peak positions from fitting as shown in the right section for an EDC at $\bar{\Gamma}$.

The top section of each panel shows a cut along k_x (MDC) at E_F . The strongest feature is a small pocket “ a ” at the \bar{B} point just below E_F . A second Fermi surface feature “ b_1 ” shows two Fermi crossings at $k_x=0.32$ \AA^{-1} and 0.4 \AA^{-1} , together with its symmetry-related copies. It consists of two parallel dispersing bands with a splitting of ≈ 100 meV. The third feature “ c ” is a completely occupied band with a band apex at $\bar{\Gamma}$. Two copies with parallel dispersions may again be distinguished, although the relative intensities differ strongly. The left section of Fig. 2(b) shows an EDC at $\bar{\Gamma}$, where the two peaks due to this band are highlighted by the resulting Lorentzian functions from peak fitting. The peak positions from this fitting procedure are marked as dots in the panel. The splitting is ≈ 100 meV at $\bar{\Gamma}$ and increases to almost 200 meV at the lower band apex.

An orthogonal map through $\bar{\Gamma}$ in the direction of \bar{Y} is shown in Fig. 3. Feature “ c ” is again visible as a double peak (EDC in the right section of the figure). The most prominent feature “ b_2 ” is a steeply dispersing band with a Fermi crossing at $k_y=0.15$ \AA^{-1} . Due to the strong intensity differences of the two parallel dispersing copies, its splitting is revealed only by careful peak fitting as shown on the top part of the figure for an MDC at E_F and by tracing the same band along the Fermi surface.

The Fermi surface map (Fig. 4) was measured by acquiring dispersion panels at various tilt angles away from the high-symmetry plane. The intensity at E_F was extracted by integrating over a window of 40 meV around E_F . The two panels of Fig. 4 were thus measured with orthogonal photon polarizations as indicated. The data were not symmetrized or distorted. At $T=200$ K, the electronic structure is still unaffected by the CDW transition^{5,6} and the Fermi surface is representative of the unmodulated high-temperature unit cell.

The locus of features “ a ,” “ b_1 ,” and “ b_2 ” is indicated in the Fermi surface map in Fig. 4. The identification of these features enables us to attribute feature a to the small electron pocket of the q1D Fermi surface. The intensity is seen as a wide band on both sides of the BZB. Features b_1 and b_2 form the more corrugated 3D Fermi surface.

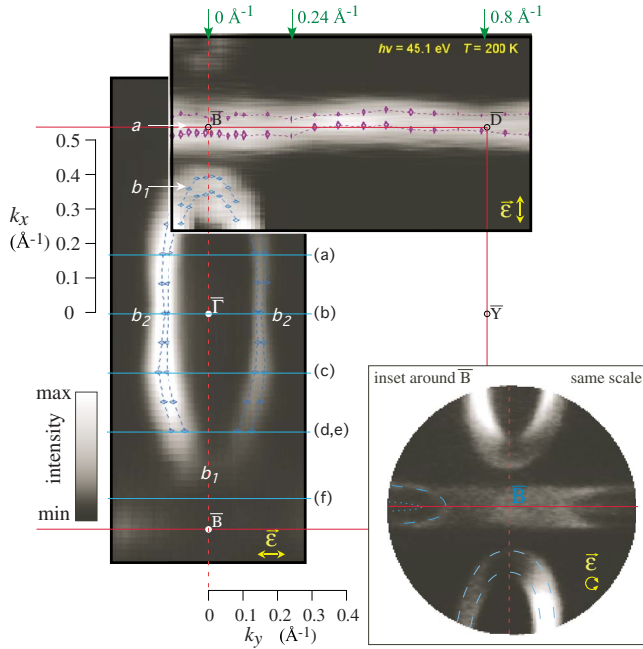


FIG. 4. (Color online) Fermi surface map of ZrTe_3 as measured by ARPES at $h\nu=45.1$ eV and $T=200$ K. The crystal symmetry is indicated by the 2D Brillouin zone boundaries. The features marked “a,” “ b_1 ,” and “ b_2 ” correspond to Figs. 2 and 3. The two panels have been measured with linearly polarized light in different directions as indicated by arrows. Markers show the position of MDC peak fits. Horizontal lines (a)–(f) correspond to cuts shown in Fig. 5 and arrows at the top to Fig. 7. The inset shows a higher resolution data set around \bar{B} acquired using elliptically polarized light.

The pocket of intensity of the q1D sheet (feature *a*) is visible all along the line $\bar{B}-\bar{D}$. The center between the two MDC peak positions forms a slightly curved line although it should follow the straight line of the BZB. We assign this artificial curvature to slight motions of the beam spot as the sample is rotated. The observation of a dispersion (see also Fig. 7 below) allows the determination of the two peak positions of the Fermi wave vectors from the MDCs. The inset displaying high-resolution data around \bar{B} reveals that at least one Fermi surface sheet in the q1D pocket does not reach all the way to the \bar{B} point as a closing arc is visible. However, a high intensity is seen in a region everywhere along the BZB including \bar{B} . Inside the closing Fermi arc, a sharp second sheet is visible and marked as a dotted line. This band is again visible in the dispersion plot in Fig. 7(b).

The 3D sheet (b_1 and b_2) has the shape of a flattened oval. The splitting leads to two concentric copies. The momentum splitting at location b_2 is reduced to almost zero. This is due to the steep dispersion of the band as seen in Fig. 3. The splitting becomes readily visible in its evolution along the Fermi surface as shown in Fig. 5. The MDCs in the top sections (a)–(d) are well described by peak fitting four Lorentzian peaks of equal width. In panels (e) and (f) showing maps along k_y for values of k_x where the FS sheet closes, peak fitting was performed on the EDCs, identifying two parallel copies of the band and allowing a splitting of 120–180 meV to be determined. Note that panel (f) corresponds to the occupied part of feature b_1 in Fig. 2. The intensities

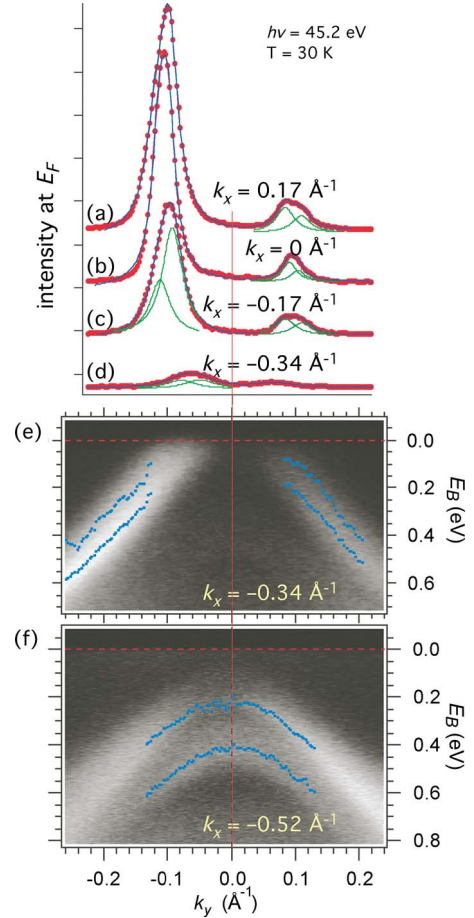


FIG. 5. (Color online) (a)–(d) Momentum distribution curves at E_F for cuts parallel to k_y at various k_x as indicated by horizontal lines in Fig. 4. Solid lines are the resulting curves from peak fitting. (e) and (f) ARPES dispersion maps parallel to k_y at k_x as indicated. The peak positions from peak fitting are marked by dots. Map (e) coincides with curve (d).

vary due to the different directions of the polarization of the light. In particular the contrast to another band obscuring the view in Fig. 2 is greatly enhanced.

IV. ORIGIN OF THE SPLITTING

The splitting of both the band “c” at $\bar{\Gamma}$ and of the 3D Fermi surface by 100–200 meV is not expected in the bulk electronic structure. Both bands are derived from highly directional Te *p* orbitals with some hybridization with Zr *d* states.¹² The low-symmetry crystal structure does not permit a degeneracy of these bands (except for the Kramers degeneracy due to the inversion symmetry, which forces spin up and spin down to be degenerate). Possible explanations of a splitting of this order of magnitude include (i) ferromagnetic symmetry breaking leading to an exchange splitting or (ii) spin-orbit (SO) splitting of the kind found in the closed *p*-shells of atoms. The former (i) would require the sample to be ferromagnetic, which has not been observed. The latter (ii) was proposed by Pacile *et al.* in the related ZrSe_3 , HfSe_3 , and ZrS_3 .⁸ In these semiconducting systems a band at $\bar{\Gamma}$ is

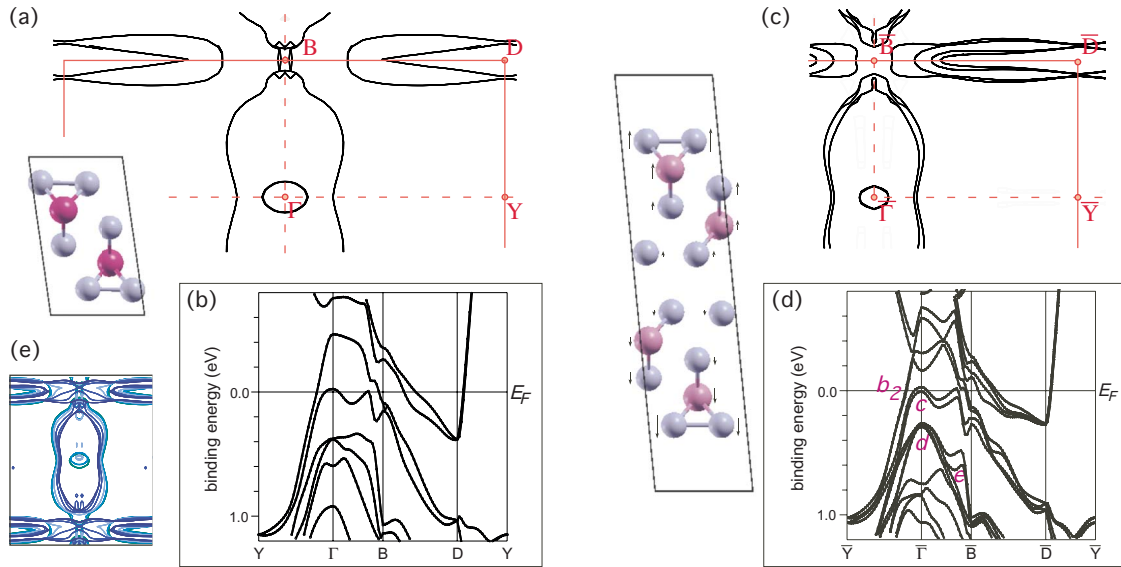


FIG. 6. (Color online) Fermi surface and band-structure calculations of (a) and (b) bulk ZrTe_3 and (c) and (d) a two-layer slab of slightly distorted ZrTe_3 . The unit cells for the *ab initio* are shown schematically. In the slab unit cell, the displacements with respect to the bulk configuration are indicated by arrows. The inset (e) shows overlaid bulk Fermi surfaces for different values of c^* from Γ -Z (effect of k_{\perp} broadening).

observed in ARPES spectra that disperses like feature c in our data and shows a similar splitting. The arguments in favor of SO splitting are (a) the order of magnitude of the splitting which matches atomic expectation for the chalcogenide p shell and (b) an increase in the splitting in the selenide compared to the sulphide. This splitting would require, however, that the underlying band has a degeneracy which could be lifted by the SO interaction. Other origins of the splitting could be of a geometric nature, such as (iii) bilayer splitting or (iv) inhomogeneity of the surface leading to a superposition of features from differently cleaved or clean and dirty portions. We exclude this last possibility (iv) since the splitting and intensity ratios of the features were observed reproducibly on various cleaves in different sample orientations and in different laboratories.

In order to further identify the character of the observed bands, we performed a first-principles band-structure calculation. The result of the Fermi surface and band dispersion of bulk ZrTe_3 in the a^*-b^* plane are shown in Figs. 6(a) and 6(b). The agreement of this calculation and the experiment is rather poor, although we may assign most of the bands. Feature “ d ” at Γ and the 3D Fermi surface are readily identified as the band at 0.6 eV binding energy (in agreement with the data) and the large hole pocket extending in the Γ -B direction, respectively. The q1D Fermi surface is found over a large portion along the BZ from B-D and consists of two sheets due to the two inequivalent atoms which form the Te-Te chains. The band c is assigned to the hole pocket around Γ , thus incorrectly crossing the Fermi level. Such a small pocket with few carriers could easily be an artifact of the calculation and has little significance for the total energy. The calculations were performed using a scalar-relativistic treatment of the SO interaction, thus any degeneracy lifting due to the SO energy should be visible in the calculation. Overall, the agreement of this theory with the experiment is

so poor that even a precise assignment of all bands is hard to achieve.

Having ruled out SO-splitting by the calculations, we are left with scenario (iii), a bilayer splitting. However, the inversion symmetric bulk structure does not allow such a splitting either. We must therefore assume a rearrangement of the atomic structure in the surface region probed in the photoelectron experiment (elastic escape depth ≈ 20 Å, i.e., two unit-cell heights). A lateral surface reconstruction was not observed in low-energy electron diffraction (LEED). Thus only a relaxation in the out-of-plane direction could modify the atomic positions. Such a relaxation is usually not assumed in van der Waals layered structures, as the removal of an adjacent layer leads to only a small change in the forces acting on the surface atoms.

We construct a model slab unit cell by the following considerations: a) the relaxation of the surface atoms can be investigated when we introduce a vacuum layer on one side of the double-chain Zr_2Te_6 layer, while keeping the next layer in place. b) The observation of a doubling of all bands in the data can be modeled by doubling the number of atoms in the unit cell. The simplest model that incorporates these two features consists of a super cell that doubles the layers in the c direction, while keeping the lateral periodicities in the a and b directions unchanged. A vacuum layer of five atomic units is introduced on either side of this bilayer to allow the surface atoms to relax away from their initial bulk-terminated positions. This slab unit cell is again inversion symmetric, but the two ZrTe_3 chains of the double layer are now inequivalent. The atomic positions are relaxed in the cell using standard molecular-dynamics methods in WIEN2K. This leads to a widening of the layers and the two layers move slightly apart as shown schematically by arrows in Fig. 6(d). The electronic structure in this stable configuration is strictly two dimensional.

The calculated Fermi surface (FS) and band structure of the bilayer are shown in Figs. 6(c) and 6(d). The 3D FS sheet is split into two concentric sheets. The q1D FS sheets now consist of four sheets, all of which are parallel to B-D and fulfill good nesting conditions. The small hole pocket around $\bar{\Gamma}$ still appears in the calculation, but the dispersion reveals that only one of the split bands is slightly unoccupied. The splitting in this calculation was introduced by construction (doubling of the number of atoms). However, the inspection of the features reveals the following improvement of the match with the data: Feature “*d*” and the hooklike feature “*e*” close to B are found in this calculation while the bulk calculation shows a monotonic down dispersion of the corresponding band (cf. Figure 2). The splitting of feature *c* at $\bar{\Gamma}$ is seen in the calculation, although it is smaller (50 meV) than that observed experimentally (100 meV). In agreement with the experiment, the splitting increases to about twice this value along the dispersion $\bar{\Gamma}$ - \bar{B} . The splitting of the 3D Fermi surface is well-reproduced in this calculation as well as the closure before reaching the B point.

A more realistic model of the surface would consist of a semi-infinite arrangement of Zr_2Te_6 double layers in the bulk configuration up to the second to last double layer. The last layer would then relax and rearrange in the fashion found in our bilayer model [arrows in Fig. 6(c)]. This model or a slab model including inner layers to model the bulk is, however, beyond the capacities of our current computer systems and would lead to the appearance of many close-laying bands for the almost equivalent layers, unless a significant relaxation is introduced like in our relaxed bilayer model. We find that our simple bilayer model captures most of the features in the data and conjecture that an effective bilayer situation is established within relaxed outermost double layer. A deeper-reaching long-range reconstruction would rather lead to a smearing of the observed structures, while a clear splitting of sharp sub-bands is observed.

Also, the momentum broadening of the photoemission experiment due to the surface would lead to a smearing rather than a splitting. This is illustrated in Fig. 6(e), where cuts of the bulk Fermi surface parallel to the Γ -B-D-Y plane are superimposed. A k_{\perp} broadening of the photoelectron momentum would correspond to a smearing of the Fermi surface contours around some center value of k_{\perp} given by the center of the k_{\perp} distribution. This central k_{\perp} is expected to change with photon energy even if we don't know its value. We have, however, observed the same splitting into the same pair of sub-bands at all measured photon energies with only the relative intensity of the features changing and therefore we rule out a significant effect of k_{\perp} broadening. Note that a three-dimensional dispersion and Fermi surface were observed in similarly layered transition-metal dichalcogenides.^{17,18}

We thus consider a surface-relaxed structure of the top double Zr_2Te_6 layer. Our spectroscopic data cannot give a direct structural determination of this layer, but the agreement of many observed features greatly improved by a bilayer model that includes relaxation due to the removal of the next layer at the surface. Spin-orbit splitting as the origin of the splitting is ruled out due to the fact that the bulk bands

in question are nondegenerate in the low-symmetric structure.

V. CDW GAP

Bearing in mind that the photoemission experiment probes a modified surface arrangement of the atoms we can proceed to inspecting the opening of a gap in the electronic structure due to the charge density wave formation. The gap of ZrTe_3 has previously been observed,^{5,7} but only as a reduction in spectral weight at the Fermi level within the intensity on the BZB. The dispersion of the electron band could not be resolved. The higher resolution of the spectrometers used in the current study allows the band to be seen as a parabolic dispersion along k_x for all sections along \bar{B} - \bar{D} . As the temperature is lowered and spectral weight is shifted away from the Fermi level, the band dispersions remain traceable up to E_F , although the intensity is reduced within the gap. Figure 7 shows three sections along k_x at \bar{B} [equivalent to Fig. 2(a)], near \bar{B} at $k_y=0.24 \text{ \AA}^{-1}$ and at \bar{D} . At least one electronlike band is observed at \bar{B} , two at $k_y=0.24 \text{ \AA}^{-1}$ and again one at \bar{D} .

The Fermi surface is thus partially gapped, leaving ample sheets for both metallic conductivity below T_{CDW} and superconductivity. The 3D sheet does not show any change with temperature, the q1D sheet has a fully developed gap in a large region around \bar{D} . On approaching \bar{B} , the gap is reduced and no gap is seen for $k_y < 0.2 \text{ \AA}^{-1}$. The inset of Fig. 4 shows a closing arc of one sheet of the FS at $k_y=0.16 \text{ \AA}^{-1}$. At B a high intensity is, however, still present. We assign this intensity to another FS sheet that is not identified by the calculations. This FS sheet at \bar{B} deserves special attention as Yokoya *et al.*⁵ have found a strong increase in spectral weight close to E_F at low temperature in this position. Our data show a band at \bar{B} with a dispersion along k_x [Figs. 7(a) and 7(e)]. The band is not observed when the photon polarization is along b^* (see Fig. 4), thus it is odd with respect to the b^* - c^* plane. It was suggested that a van Hove singularity (vHs) could be present at this point at E_F due to the fact that the 3D and q1D FS sheets touch each other.^{12,13} However, the Fermi surface sheets do not touch at B, with the 3D sheets closing at $k_x=0.32 \text{ \AA}^{-1}$ and $k_x=0.4 \text{ \AA}^{-1}$, respectively, for the two split sheets, at a safe distance from the B-point ($k_x=0.55 \text{ \AA}^{-1}$). Our calculations do not predict a Fermi surface sheet at \bar{B} and cannot assign the observed band. Thus the origin of the sharp peak observed by Yokoya *et al.* at low temperatures requires further studies.

In the region $k_y > 0.2 \text{ \AA}^{-1}$, where the CDW gap was observed in previous studies,^{5,7} the band dispersion and intensity distribution is determined by a peak fitting analysis of the MDCs. In a large region around D, the gap is fully developed at $T=30 \text{ K}$.⁵ Surprisingly, the band dispersion remains unambiguously traceable up to E_F as shown in Figs. 7(f) and 7(g). The shift in spectral weight away from E_F is seen as a linear increase in the band intensity over a binding-energy interval of 150 meV. This compares to a constant intensity over the whole binding-energy range derived from a similar analysis at room temperature [Fig. 7(h)]. The expected back folding of the band due to the new periodicity is

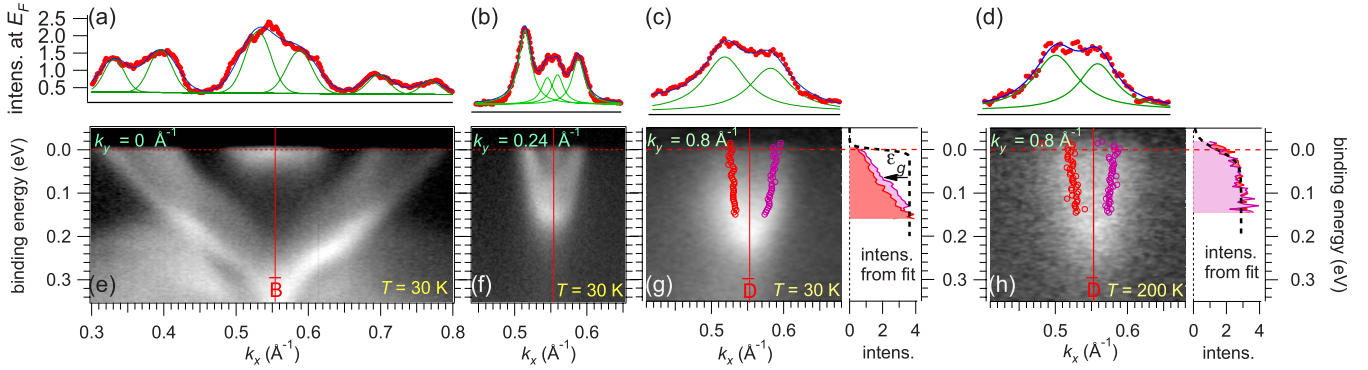


FIG. 7. (Color online) ARPES dispersion maps at three different position along the Brillouin zone boundary BZB from \bar{B} to \bar{D} at low $T=30$ K (e)–(g) and $T=200$ K (h). The Fermi wave vector on either side of the BZB is determined by peak fitting as shown in (a)–(d) of MDCs at E_F . In panels (g) and (h) the dispersion is traced by fits to the MDCs by two Lorentzians of equal width. The intensities of these fits are shown to the right of the panel together with a Fermi occupation function (dashed line) at the corresponding temperature. The half-height of the intensity curve at $T=30$ K (h) corresponds to the magnitude of the gap ε_g and is marked by an arrow. The data sets (a) and (b) and (e) and (f) were acquired with a higher resolution spectrometer and elliptically polarized light, whereas (c) and (d) and (g) and (h) were acquired with linearly polarized light.

not observed and the gap value is determined as the binding energy where the band acquires half of its maximum intensity $\varepsilon_g=65 \pm 10$ meV. An upper band apex (whose binding energy would correspond to the gap value) is not found.

ZrTe₃ is a rather special CDW system since the component $q_{CDW}^{(a^*)}=0.07$ along a^* is very small and correspondingly the wavelength of the modulation along the chains is very long ($\lambda \approx 80$ Å). This property is conserved in the cleaved surface of ZrTe₃ and we determine $2k_F=0.06$ Å⁻¹ $=0.11 \cdot a^*$, slightly larger than suggested by the bulk superstructure. This nesting suggests a CDW in the surface layer as $(\bar{q}^x, \bar{q}^y)=(0.11, 0)$. The long wavelength and the finite correlation length of the Peierls modulation, even well below the transition temperature $T_{CDW}=63$ K, lead to a smearing of the band folding in momentum space. Since the Peierls distortion only creates a slight modulation in the underlying crystal structure, it is not surprising that the back-folded band is not visible in the data. However, the removal of spectral weight from the Fermi level is still assigned to a partial CDW gapping of the Fermi surface.

VI. CONCLUSIONS

We have presented a detailed Fermi surface map and band dispersion study of ZrTe₃. The basic features of the Fermi surface, i.e., a large 3D body around $\bar{\Gamma}$ and a q1D sheet along the Brillouin zone-boundary \bar{B} – \bar{D} are consistent with previous results, but the 3D Fermi surface as well as a band at $\bar{\Gamma}$ are found to be split by 100–200 meV. This splitting is explained by a surface relaxation leading to a bilayer splitting of the electronic structure.

The q1D FS sheets are seen all along the BZB \bar{B} – \bar{D} . The band is traceable by peak fitting with a Fermi wave vector $2k_F=0.06$ Å⁻¹. This opening of the electron pocket is seen everywhere along the BZB, although at least one sheet of the Fermi surface closes in an arc at $k_y=0.15$ Å⁻¹. A second sheet is identified inside the nested sheet and at \bar{D} they are degenerate. Very good nesting conditions are therefore found

all along \bar{B} – \bar{D} . The CDW gap is identified as a shift in spectral weight away from E_F in a gap of $\varepsilon_g=65 \pm 10$ meV for $k_y > 0.2$ Å⁻¹. This gap is not seen as a back-folded band, due to the long wavelength and finite correlation length of the Peierls distortion.

This leads to the conclusion that the surface of ZrTe₃, as well as other MX₃ systems, does not have a simple bulk termination. Even though the crystal probably cleaves in the van der Waals bonded gap between Te layers and the surface termination has no dangling bonds, the outermost layer relaxes into a configuration which is slightly different from the situation in the bulk. The electronic levels of this surface system split in a fashion similar to a bilayer splitting. All observations by highly surface-sensitive techniques, in particular the VUV ARPES studies performed by Yokoya *et al.*, Starowicz *et al.*, and Pacile *et al.* (Refs. 5, 7, and 8), and probably also the studies on NbSe₃ by Schäfer *et al.*,¹⁹ have therefore probed a special surface system of reconstructed MX₃ chains, which closely resembles the bulk but is slightly modified. Since a small modification of the atomic arrangement can drastically influence the CDW, this opens up the possibility to deliberately manipulate the CDW material on its surface and thus study the CDW phase transition in new and controlled systems.

ACKNOWLEDGMENTS

We would like to thank A. Chainani and T. Yokoya for help at the start of experiments. We have gratefully used data analysis routines from A. Ino, M. Miura, and F. Baumberger. Inspiring discussions of the data and calculations are acknowledged with M. Grioni, J. Osterwalder, L. Patthey, and P. Aebi. We thank W. Welnic for repeating some of the calculations for confirmation and A. Petrovic for careful reading of the manuscript. The experiment was performed at the Hiroshima Synchrotron Radiation Centre (Proposal No. 06-A-17) with additional data acquired at the Surface and Interface Spectroscopy beamline at the Swiss Light Source. *Ab initio*

calculations were performed using the WIEN2K package. One of us (M.H.) would like to thank the Japanese Society for the Promotion of Science (JSPS) for financial support. Support

by the Fonds National Suisse pour la Recherche Scientifique through Div. II and the Swiss National Center of Competence in Research MaNEP is gratefully acknowledged.

*Present address: Diamond Light Source, Harwell Campus, Didcot OX11 0DE, United Kingdom; moritz.hoesch@diamond.ac.uk

†Present address: Swiss Light Source, Paul Scherrer Institut, 5232 Villigen PSI, Switzerland.

¹G. Grüner, *Density Waves in Solids*, Frontiers in Physics Vol. No. 89 (Perseus Publishing, Cambridge MA, 1994).

²H. W. Yeom, S. Takeda, E. Rotenberg, I. Matsuda, K. Horikoshi, J. Schaefer, C. M. Lee, S. D. Kevan, T. Ohta, T. Nagao, and S. Hasegawa, *Phys. Rev. Lett.* **82**, 4898 (1999).

³J. Schäfer, C. Blumenstein, S. Meyer, M. Wisniewski, and R. Claessen, *Phys. Rev. Lett.* **101**, 236802 (2008).

⁴R. Yomo, K. Yamaya, M. Abliz, M. Hedo, and Y. Uwatoko, *Phys. Rev. B* **71**, 132508 (2005).

⁵T. Yokoya, T. Kiss, A. Chainani, S. Shin, and K. Yamaya, *Phys. Rev. B* **71**, 140504(R) (2005).

⁶A. Perucchi, C. Sondergaard, S. Mitrovic, M. Grioni, N. Barisic, H. Berger, L. Forro, and L. Degiorgi, *Eur. Phys. J. B* **48**, 489 (2004).

⁷P. Starowicz, C. Battaglia, F. Clerc, L. Despont, A. Prodan, H. van Midden, U. Szerer, A. Szytula, M. Garnier, and P. Aebi, *J. Alloys Compd.* **442**, 268 (2007).

⁸D. Pacile, M. Papagno, M. Lavagnini, H. Berger, L. Degiorgi, and M. Grioni, *Phys. Rev. B* **76**, 155406 (2007).

⁹S. Takahashi, S. Sambongi, and S. Okada, *J. Phys. (Paris), Colloq.* **C3**, 1733 (1983).

¹⁰D. J. Eaglesham, J. W. Steeds, and J. A. Wilson, *J. Phys. C* **17**, L697 (1984).

¹¹M. Hoesch, A. Bosak, D. Chernyshov, H. Berger, and M. Krisch, *Phys. Rev. Lett.* **102**, 086402 (2009).

¹²C. Felser, E. Finckh, H. Kleinke, and W. Tremel, *J. Mater. Chem.* **8**, 1787 (1998).

¹³K. Stöwe and F. Wagner, *J. Solid State Chem.* **138**, 160 (1998).

¹⁴Y. Kubo, Y. Sakurai, M. Ito, A. Koizumi, K. Yamaya, and Y. Uwatoko, *J. Phys. Soc. Jpn.* **76**, 064711 (2007).

¹⁵K. Shimada, M. Arita, T. Matsui, K. Goto, S. Qiao, Y. Yoshida, M. Taniguchi, H. Namatame, T. Sekitani, K. Tanaka, H. Yoshida, K. Shirasawa, N. Smolyakov, and A. Hiraya, *Nucl. Instrum. Methods Phys. Res. A* **467**, 504 (2001).

¹⁶P. Blaha, K. Schwarz, G. Madsen, D. Kvasnicka, and J. Luitz, *An Augmented Plane Wave Plus Local Orbitals Program for Calculating Crystal Properties* (Technische Universität Wien, Austria, 2001).

¹⁷K. Rossnagel, L. Kipp, M. Skibowski, C. Solterbeck, T. Strasser, W. Schattke, D. Voss, P. Kruger, A. Mazur, and J. Pollmann, *Phys. Rev. B* **63**, 125104 (2001).

¹⁸V. N. Strocov, E. E. Krasovskii, W. Schattke, N. Barrett, H. Berger, D. Schrupp, and R. Claessen, *Phys. Rev. B* **74**, 195125 (2006).

¹⁹J. Schäfer, M. Sing, R. Claessen, E. Rotenberg, X. J. Zhou, R. E. Thorne, and S. D. Kevan, *Phys. Rev. Lett.* **91**, 066401 (2003).